Biomedical Engineering Letters (2019) 9:189–201
https://doi.org/10.1007/s13534-019-00098-9

ORIGINAL ARTICLE

Constitutive law of healthy gallbladder walls in passive state with damage effect

Wenguang Li[1]

Received: 27 October 2018 / Revised: 14 January 2019 / Accepted: 16 January 2019 / Published online: 6 February 2019

Abstract
Biomechanical properties of human gallbladder (GB) wall in passive state can be valuable to diagnosis of GB diseases. In the article, an approach for identifying damage effect in GB walls during uniaxial tensile test was proposed and a strain energy function with the damage effect was devised as a constitutive law phenomenologically. Scalar damage variables were introduced respectively into the matrix and two families of fibres to assess the damage degree in GB walls. The parameters in the constitutive law with the damage effect were determined with a custom MATLAB code based on two sets of existing uniaxial tensile test data on human and porcine GB walls in passive state. It turned out that the uniaxial tensile test data for GB walls could not be fitted properly by using the existing strain energy function without the damage effect, but could be done by means of the proposed strain energy function with the damage effect involved. The stresses and Young moduli developed in two families of fibres were more than thousands higher than the stresses and Young's moduli in the matrix. According to the damage variables estimated, the damage effect occurred in two families of fibres only. Once the damage occurs, the value of the strain energy function will decrease. The proposed constitutive laws are meaningful for finite element analysis on human GB walls.

Keywords Gallbladder · Constitutive law · Damage variable · Biomechanical property · Strain energy function · Yield point

1 Introduction

The gallbladder (GB) lies on the visceral surface of the liver, and a thin-walled distensible and contractible sac [20], see Fig. 1. It stores and concentrates the bile, when one is in fasting, but discharges it into the small intestine, when one is consuming meal or in drinking. GBs can suffer from a variety of disease such as gallstones, cholecystitis, acalculous gallbladder disease, biliary dyskinesia and gallbladder cancer [2, 15, 29]. The disease can alter passive and active biomechanical properties of GB wall [1, 4, 7, 12, 25]. Thus, the biomechanical properties of GB wall should be valuable to diagnosis of GB diseases. Unfortunately, such an issue has been rarely documented in literature so far, especially for the passive biomechanical property.

Currently, there are a few measurements on biomechanical properties of GB wall. GB pressure–volume curves were measured in vitro by inflating the GB with saline in passive and active states [5, 6, 18, 19, 21, 27, 28]. It was shown that GB pressure–volume curves exhibited visco-elastic property [6, 18, 19, 21, 28]. The compliance of GB was estimated from experimental data [28].

Porcine GB walls were measured under compression loads on a material testing machine and engineering stress–strain curves were established in passive compressed state [26].

An organ inflating experimental set-up was built and a lamb GB shape was recorded in vitro optically when the GB was pressurized with phosphate-buffered solution in Genovese et al. [11]. Based on membrane mechanics model, the passive biomechanical property constants were decided numerically with finite element analysis (FEA).

Porcine GBs were harvested from a slaughterhouse and subject to indentation experiments along the circumferential and longitudinal directions when the GBs chamber was full of bile. Then the GBs were cut into specimens in both the directions; finally, these specimens were elongated in passive state on a uniaxial material testing machine [32]. The GB wall material property constants could be determined

✉ Wenguang Li
Wenguang.Li@Glasgow.ac.uk

[1] School of Mathematics and Statistics, University of Glasgow, Glasgow G12, 8QQ, UK

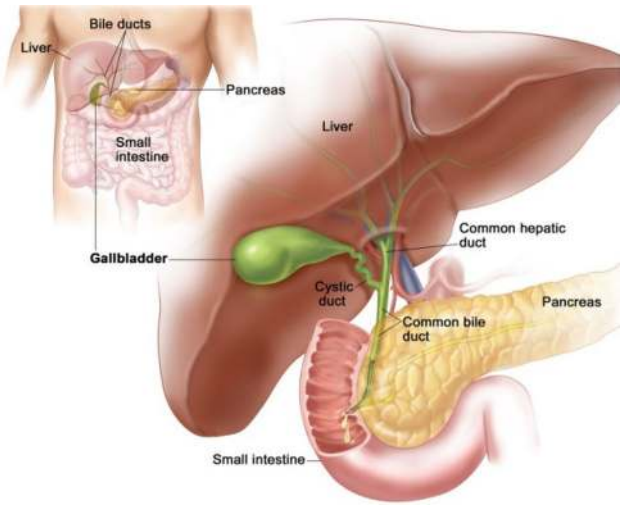

Fig. 1 The gallbladder, and its tract, the picture is from: https://healthjade.com/gallbladder/

based on the indentation experimental data and strain energy function proposed by Fung et al. [10].

Passive uniaxial biomechanical property of human GB walls was identified experimentally on a material testing machine in Karimi et al. [14] based on a few specimens harvested from the GBs of corpses in hospital. The engineering stress–strain curves were provided.

Currently, there is no constitutive law for GB walls in passive state based on uniaxial tensile testing data; consequently FEA on nonlinear anisotropic GB walls has been limited so far.

In the paper, two constitutive laws with damage effect were established based on the uniaxial tensile test data on human [14] and porcine [32] GB walls in passive state. Firstly, the constitutive law for passive human GB wall without damage effect in the tissue was proposed in Li et al. [22] based on the law for passive arterial walls in Holzapfel et al. [13] was used to fit the uniaxial tensile test data on human [14] and porcine [32] GB walls, and poor fitting results were encountered and the question was raised, i.e. there may be damage effect in the tissue. Secondly, to identify this effect, the instant Young's moduli of the circumferential and longitudinal specimens were estimated based on their experimental stress-stretch curves by using 6th-order polynomial and least squares method, and yield points were predicted. Thirdly, the corresponding extra terms for the damage effect were involved in the constitutive model in Li et al. [22] for GB walls according to the idea in Li and Luo [23], then the model parameters were inversely determined by using these experimental data with a MATLAB code. Finally, scalar damage variables were defined respectively for the matrix and two families of fibres to evaluate the damage degree in the walls and a constitutive law was finalised and discussed.

This idea is original and has not been documented in literature, thus the proposed and determined constitutive laws are meaningful for FEA on human GB walls, but also are significant in biomedical engineering and biomechanics.

2 Experimental data

Uniaxial tensile tests on five pairs of the circumferential and longitudinal specimens of porcine GB wall were conducted by Xiong et al. [32] and the engineering stresses were presented in terms of stretch. It turned out that the circumferential samples were stiffer than the longitudinal one in stress-stretch curves. The experimental set-up and measured Cauchy stress-stretch curves are illustrated in Fig. 2a and c.

Sixteen GBs were excised from the cadavers of human subjects with 69.3 ± 9.8 years old and GB wall specimens were cut along the axial and transversal directions and tested on DBBP-50 material testing machine (Bongshin Co. Korea) by Karimi et al. [14]. Unfortunately, in Karimi et al. [14], the axial and transversal directions were unclear in the text and figures. Here, it is assumed that the axial direction is the longitudinal direction, while the transversal direction is the circumferential direction in common sense. The stress value seems to be larger by one order than the porcine GB wall in tension [32] and in compression [26] because there might be something wrong in data reduction in Karimi et al. [14]. Therefore, the experimental stress values have to be reduced by 1/10 factor to make them comparable with the stress values of the porcine GB wall.

The experimental apparatus and Cauchy-stretch curves are presented in Fig. 2b and c. The experimental set-up and specimen sizes in Karimi et al. [14] are bigger than those in Xiong et al. [32]. There may exist scale effect in two experiments. In addition, the longitudinal stress-curve is stiffer than the circumferential one [14]. Two sets of the Cauchy-stretch curves in Fig. 2c will be used to establish passive constitutive laws of GB walls.

3 Constitutive laws

3.1 The raised question

A constitutive law for passive human GB wall without damage effect in the tissue was proposed in Li et al. [22] based on the law for passive arterial walls in Holzapfel et al. [13]. This strain energy function based constitutive law is written as

$$\psi = c\left(I_1 - 3\right) + \frac{k_1}{2k_2}\left[e^{k_2(I_4-1)^2} - 1\right] + \frac{k_3}{2k_4}\left[e^{k_4(I_6-1)^2} - 1\right] \quad (1)$$

where c is the matrix material stiffness, k_1 and k_2 are the initial stiffness and its change rate with stretch of the circumferential fibres, k_3 and k_4 are the initial stiffness and its change

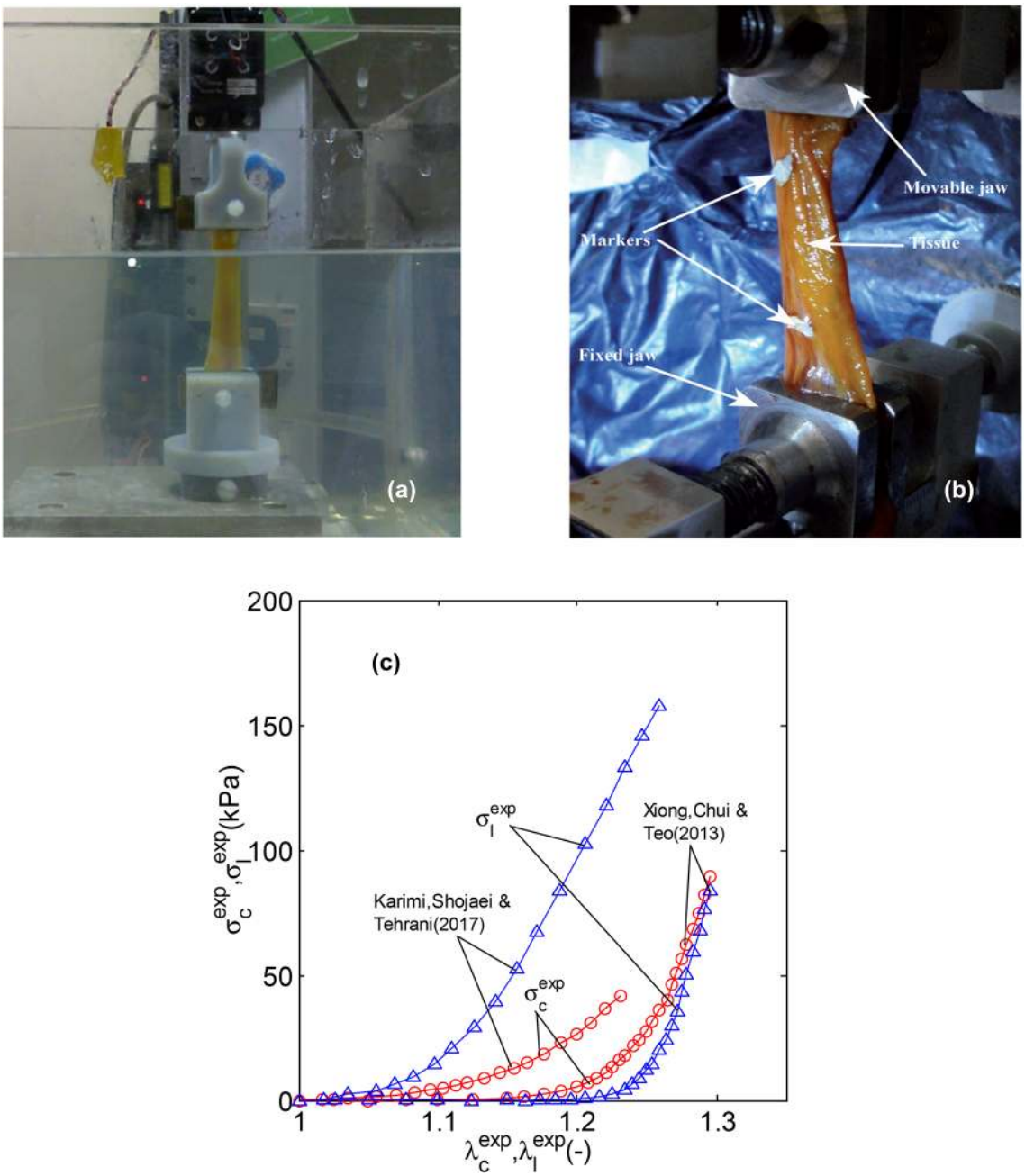

Fig. 2 Experimental set-up and tensile testing results of GB wall samples, **a** wet tensile testing apparatus in Xiong et al. [32], **b** dry tensile testing machine in Karimi et al. [14], **c** the measured Cauchy stress-stretch curves of porcine [32], and human [14] GB walls

rate with stretch of the longitudinal fibres, I_1 is the trace of the Cauchy–Green deformation tensor, $I_1 = \lambda_c^2 + \lambda_l^2 + \lambda_h^2$, λ_c ,λ_l and λ_h are the stretches in the circumferential, longitudinal and thickness directions, respectively, I_4 is the squared λ_c, $I_4 = \lambda_c^2$, and I_6 is the squared λ_l, $I_6 = \lambda_l^2$.

Five model parameters c, k_1, k_2, k_3 and k_4 can be determined based on the experimental stress-stretch curves shown in Fig. 2c by using *lsqnonlin* function in MATLAB in terms of "trust-region-reflective" optimization algorithm to minimize the value of the following objective function

$$f(c, k_1, k_2, k_3, k_4) = \sum_{i=1}^{n_c} \left(\sigma_{ci}^{\text{mod}} - \sigma_{ci}^{\text{exp}}\right)^2 + \sum_{j=1}^{n_l} \left(\sigma_{lj}^{\text{mod}} - \sigma_{lj}^{\text{exp}}\right)^2 \quad (2)$$

where σ_{ci}^{mod} and σ_{lj}^{mod} are the circumferential and longitudinal Cauchy stresses calculated by using the strain energy function in Eq. (1) at the ith experimental stretch $\lambda_{ci}^{\text{exp}}$ in the

uniaxial tensile test of a circumferential sample and at the jth experimental stretch $\lambda_{lj}^{\exp}$ in the similar test of a longitudinal sample, respectively; n_c and n_l are the total numbers of experimental points in the uniaxial tensile tests on the circumferential and longitudinal samples; σ_{ci}^{exp} and σ_{lj}^{exp} are the measured circumferential and longitudinal Cauchy stresses at the ith and jth experimental points, and presented in Fig. 2c.

$\sigma_{ci}^{\mathrm{mod}}$ and $\sigma_{lj}^{\mathrm{mod}}$ are calculated by the following equations when the incompressible condition $\lambda_c\lambda_l\lambda_h = 1$ is held in the GB wall. For the uniaxial tensile test of circumferential samples, $\sigma_{ci}^{\mathrm{mod}}$ is read as

$$\begin{aligned}\sigma_{ci}^{\mathrm{mod}} &= \lambda_{ci}^{\exp}\frac{\partial\psi}{\partial I_1}\frac{\partial I_1}{\partial\lambda_c}\bigg|_{\lambda_c=\lambda_{ci}^{\exp}} + \lambda_{ci}^{\exp}\frac{\partial\psi}{\partial I_4}\frac{\partial I_4}{\partial\lambda_c}\bigg|_{\lambda_c} \\ &= \lambda_{ci}^{\exp}, I_1 = \lambda_c^2+\lambda_l^2+\lambda_h^2, \lambda_l = \lambda_h = 1/\lambda_c\end{aligned} \tag{3}$$

and, for the uniaxial tensile test of longitudinal samples, $\sigma_{lj}^{\mathrm{mod}}$ is expressed as

$$\begin{aligned}\sigma_{lj}^{\mathrm{mod}} &= \lambda_{lj}^{\exp}\frac{\partial\psi}{\partial I_1}\frac{\partial I_1}{\partial\lambda_l}\bigg|_{\lambda_l=\lambda_{lj}^{\exp}} + \lambda_{lj}^{\exp}\frac{\partial\psi}{\partial I_6}\frac{\partial I_6}{\partial\lambda_l}\bigg|_{\lambda_l=\lambda_{lj}^{\exp}}, I_1 \\ &= \lambda_c^2+\lambda_l^2+\lambda_h^2, \lambda_c = \lambda_h = 1/\lambda_l\end{aligned} \tag{4}$$

The standard deviation error in the Cauchy stress is calculated to evaluate the curve fitting quality quantitatively, the expression for the error is read as

$$\varepsilon = \frac{1}{\sigma_{mean}^{\exp}}\sqrt{\frac{\sum_{i=1}^{n_c}\left(\sigma_{ci}^{\mathrm{mod}}-\sigma_{ci}^{\exp}\right)^2+\sum_{j=1}^{n_l}\left(\sigma_{lj}^{\mathrm{mod}}-\sigma_{lj}^{\exp}\right)^2}{n_c+n_l}}\times 100\% \tag{5}$$

where $\sigma_{mean}^{\exp}$ is the mean Cauchy stress in both kinds of uniaxial tensile test, i.e. $\sigma_{mean}^{\exp} = \left(\sum_{i=1}^{n_c}\sigma_{ci}^{\exp}+\sum_{j=1}^{n_l}\sigma_{lj}^{\exp}\right)\Big/\left(n_c+n_l\right)$.

The equations above were programmed in MATLAB, and the corresponding custom program is described in detail in the "Appendix". The determined five parameters are listed in Table 1, and a comparison is made in Fig. 3 between the measured and predicted stresses at the same stretch values. For both the human and the porcine GB walls, the predicted and measured Cauchy stress-stretch share different slopes clearly. As a result, the errors in the stress curves are as high as 16.0% and 11.6%, and suggesting the model presented by Eq. (1) is in a poor performance. Nevertheless, the constitutive law Eq. (1) needs to be updated.

3.2 Constitutive law with damage effect

Damage effect is related to instant change in Young's modulus of a specimen during its uniaxial tensile tests [9, 16, 30, 31]. To identify whether there is the damage effect in the

Table 1 Extracted model parameters from uniaxial tensile test data on human and porcine GB wall in passive state without damage

Damage effect	Parameter	GB wall	
		Human	Porcine
Excluded	c (kPa)	0.0182	0.0037
	k_1 (kPa)	9.1076	1.8718
	k_2 (–)	4.2018	6.7299
	k_3 (kPa)	47.0016	0.2681
	k_4 (–)	1.9348	10.8841
	ε (%)	15.9825	11.6071

experimental data shown in Fig. 2c, the scattered data points were best fitted by using a 6th-order polynomial, the Young's moduli of the curves were worked out by calculating the instant slopes of the curves such as circumferential modulus $E_c^{\exp} = d\sigma_c^{\exp}\Big/d\lambda_c^{\exp}$ and longitudinal modulus $E_l^{\exp} = d\sigma_l^{\exp}\Big/d\lambda_l^{\exp}$ and are illustrated in Fig. 4. Since the Young's modulus is very small and less change when $\lambda_c^{\exp}$ and $\lambda_l^{\exp}$ are smaller than certain values, just the parts with substantial change in instant Young's moduli are fitted and demonstrated in the figure.

For the human GB wall, the longitudinal Young's modulus $E_l^{\exp}$ is always larger than the circumferential one $E_c^{\exp}$, indicating the longitudinal specimen is stiffer than the circumferential specimen. For the porcine GB wall, however, the longitudinal specimen is not stiffer than the circumferential specimen until the stretch is 1.25.

These Young's moduli rise with increasing stretch until the peak value for both the GB walls. Beyond the point with the peak Young's modulus, the modulus starts declining, suggesting the yield point existence in the curves, see Fig. 4. Therefore, there is a damage effect in the circumferential and longitudinal specimens.

To involve the damage effect in the circumferential and longitudinal specimens phenomenologically, based on the work in Li and Luo [23], the constitutive model presented by Eq. (1) was extended by adding three extra terms and rewritten in the following form

$$\begin{aligned}\psi^{dam} = c&\left[(I_1-3)-\frac{(I_1-3)^{m+1}}{(m+1)(\zeta-3)^m}\right] \\ &+\frac{k_1}{2k_2}\left\{\exp\left[k_2(I_4-1)^2\right]-1-\frac{2k_2(I_4-1)^{n+2}}{(n+2)(\xi^2-1)^n}\right\} \\ &+\frac{k_3}{2k_4}\left\{\exp\left[k_4(I_6-1)^2\right]-1-\frac{2k_4(I_6-1)^{n+2}}{(n+2)(\xi^2-1)^n}\right\}\end{aligned} \tag{6}$$

where m, n, ξ and ζ are the phenomenological parameters to describe the damage in the GB wall, m and ζ are relevant to the matrix damage; m specifies the sharpness of the

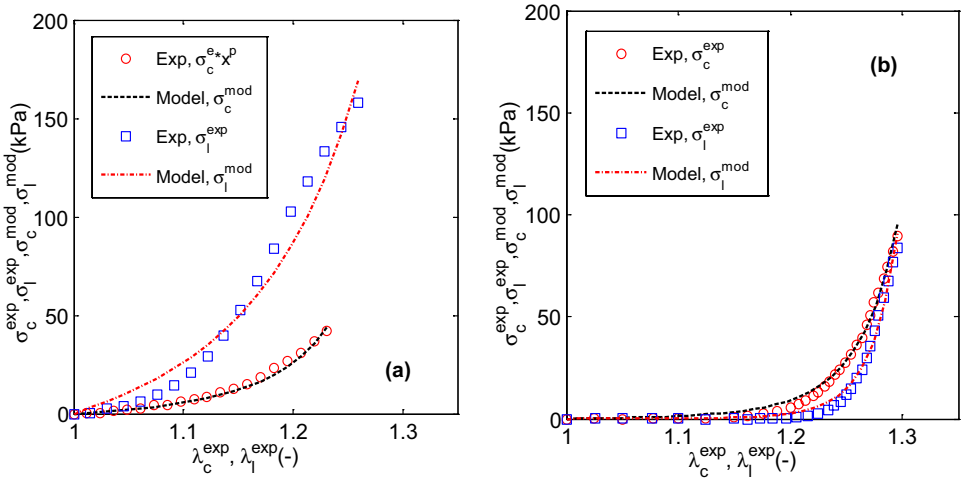

Fig. 3 The uniaxial test data and predicted Cauchy stress-stretch curves by using model Eq. (1) based on the determined parameters in Table 1, **a** human GB wall, **b** porcine GB wall

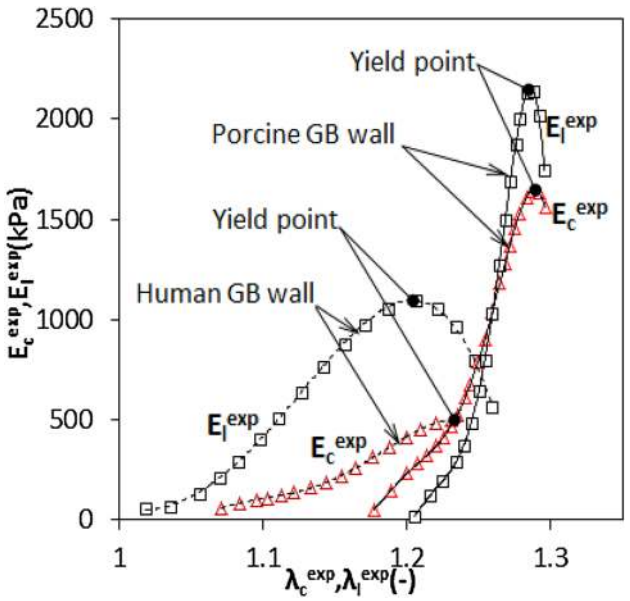

Fig. 4 The longitudinal and circumferential Young's moduli determined by fitting the uniaxial test data in Fig. 1c with 6th-order polynomial

stress-stretch curve when damage occurs, and ζ indicates the value of I_1 when the matrix damage occurs, n and ξ are the corresponding parameters for the fibre damage; n is the counterpart of m, and ξ demonstrates the fibre stretch λ_f at which the fibres damage occurs. If these parameters are chosen to be $\xi = \zeta = +\infty$ and $m = n = 1$, then the constitutive model Eq. (1) is restored.

Likewise, the uniaxial tensile test data in Fig. 2c were read into a MATLAB code to perform an optimization process and determine nine model constants c, k_1, k_2, k_3, k_4, m, n, ξ and ζ simultaneously by using same algorithm mentioned in Sect. 3.1. The decided parameters are listed in Table 2, whilst the predicted stress-stretch curves with them are plotted in Fig. 5 along with the corresponding experimental data.

Based on Tables 1 and 2, after the damage effect is considered in both specimens, the fitting errors in the stress are reduced to 4.6% and 8.2% from 16.0 and 11.6% respectively for both the GB walls.

For the porcine GB wall, the stresses are very flat as the stretch is less than 1.2 or so, suggesting just the matrix material engages in tension. However, when the stretch is in the range of 1.2–1.3, the stress level grows markedly with increasing stretch, indicating fibres are recruited extensively. This effect results in a difficulty in constitutive behaviour modelling of the porcine GB wall. Additionally, compared with the human GB wall, constants c, k_1 and k_3 are smaller, but k_2 and k_4 are larger in value.

3.3 Damage variables

In order to identify where the damage occurs in the tissue, the damage variables must be proposed and estimated. In doing so, the strain energy function in Eq. (6) is divided into three parts: the first is the strain energy function for the matrix, ψ_m^{dam}, the second is the strain energy function for the circumferential fibres, ψ_{fc}^{dam} and the third is the strain energy function for the longitudinal fibres, ψ_{fl}^{dam}, then Eq. (6) is rewritten as

$$\begin{aligned}
\psi^{dam} &= \psi_m^{dam} + \psi_{fc}^{dam} + \psi_{fl}^{dam} \\
\psi_m^{dam} &= c\left[(I_1-3) - \frac{(I_1-3)^{m+1}}{(m+1)(\zeta-3)^m}\right] \\
\psi_{fc}^{dam} &= \frac{k_1}{2k_2}\left\{\exp\left[k_2(I_4-1)^2\right] - 1 - \frac{2k_2(I_4-1)^{n+2}}{(n+2)(\xi^2-1)^n}\right\} \\
\psi_{fl}^{dam} &= \frac{k_3}{2k_4}\left\{\exp\left[k_4(I_6-1)^2\right] - 1 - \frac{2k_4(I_6-1)^{n+2}}{(n+2)(\xi^2-1)^n}\right\}
\end{aligned} \tag{7}$$

Table 2 Extracted model parameters from uniaxial tensile test data on human and porcine GB walls with damage in matrix and fibres

Damage effect	Parameter	GB wall	
		Human	Porcine
Included damage effect in matrix and fibres	c (kPa)	0.4770	0.0129
	k_1 (kPa)	5.8311	0.6444
	k_2 (–)	8.9293	10.2208
	k_3 (kPa)	23.8486	0.1964
	k_4 (–)	8.5417	12.0102
	ξ (–)	1.1825	1.2447
	n (–)	7.0763	18.6265
	m (–)	10.0174	18.5992
	ζ (–)	5.8792	4.3933
	ϵ (%)	4.5836	8.1985

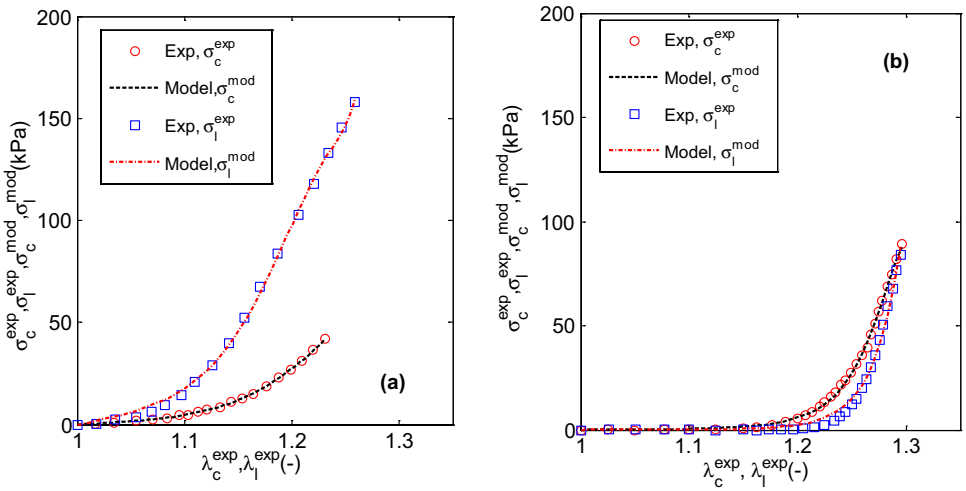

Fig. 5 The uniaxial test data and predicted Cauchy stress-stretch curves by using model Eq. (6) based on the determined parameters in Table 2, **a** human GB wall, **b** porcine GB wall

The Cauchy stress components in the tissue can be divided into three parts accordingly: the first is the stress in the matrix, σ_m^{dam}, due to ψ_m^{dam}, the second is the stress in the circumferential fibres, σ_{fc}^{dam}, and the third is the stress in the longitudinal fibres, σ_{fl}^{dam}, i.e.

$$\begin{aligned}
&\sigma_c^{dam} = \sigma_{mc}^{dam} + \sigma_{fc}^{dam}, \sigma_l^{dam} = \sigma_{ml}^{dam} + \sigma_{fl}^{dam}\\
&\sigma_{mc}^{dam} = \lambda_c \frac{\partial \psi_m^{dam}}{\partial I_1}\frac{\partial I_1}{\partial \lambda_c} = 2\left(\lambda_c^2 - 1/\lambda_c\right)\left[c - \left(\frac{I_1 - 3}{\zeta - 3}\right)^m\right]\\
&\sigma_{fc}^{dam} = \lambda_c \frac{\partial \psi_{fc}^{dam}}{\partial I_4}\frac{\partial I_4}{\partial \lambda_c} = 2\lambda_c^2 k_1 (I_4 - 1)\left[e^{k_2(I_4-1)^2} - \left(\frac{I_4 - 1}{\xi^2 - 1}\right)^n\right]\\
&\sigma_{ml}^{dam} = \lambda_l \frac{\partial \psi_m^{dam}}{\partial I_1}\frac{\partial I_1}{\partial \lambda_l} = 2\left(\lambda_l^2 - 1/\lambda_l\right)\left[c - \left(\frac{I_1 - 3}{\zeta - 3}\right)^m\right]\\
&\sigma_{fl}^{dam} = \lambda_l \frac{\partial \psi_{fl}^{dam}}{\partial I_6}\frac{\partial I_6}{\partial \lambda_l} = 2\lambda_l^2 k_3 (I_6 - 1)\left[e^{k_4(I_6-1)^2} - \left(\frac{I_6 - 1}{\xi^2 - 1}\right)^n\right]
\end{aligned} \tag{8}$$

Taking the derivatives of σ_c^{dam}, σ_{mc}^{dam} and σ_{fc}^{dam} with respect to λ_c and the derivatives of σ_l^{dam},σ_{ml}^{dam} σ_{fl}^{dam} with respective to λ_l, the Young's moduli can be calculated by using the following equations

$$\begin{aligned}
&E_c^{dam} = \partial\sigma_c^{dam}/\partial\lambda_c, E_{mc}^{dam} = \partial\sigma_{mc}^{dam}/\partial\lambda_c, E_{fc}^{dam} = \partial\sigma_{fc}^{dam}/\partial\lambda_c\\
&E_l^{dam} = \partial\sigma_l^{dam}/\partial\lambda_l, E_{ml}^{dam} = \partial\sigma_{ml}^{dam}/\partial\lambda_l, E_{fl}^{dam} = \partial\sigma_{fl}^{dam}/\partial\lambda_l
\end{aligned} \tag{9}$$

where E_c^{dam}, E_{mc}^{dam} and E_{fc}^{dam} are the circumferential Young's moduli in total, in the matrix and in the fibres; similarly, E_l^{dam}, E_{ml}^{dam} and E_{fl}^{dam} are the longitudinal Young's moduli in total, in the matrix and in the fibres. The Young's moduli in Eq. (9) are calculated numerically from the stress-stretch curves by using the 2nd-order difference scheme.

The material property in virgin/undamaged state is presented by the model parameters c, k_1, k_2, k_3 and k_4 in Table 2 which are associated with Eq. (7). In this case, the first part is the strain energy function for the matrix ψ_m^{vir}, the second part is the strain energy function for the circumferential fibres, $\psi_{\mathrm{fc}}^{\mathrm{vir}}$, and the third part is the strain energy function

for the longitudinal fibres, $\psi_{\mathrm{fl}}^{\mathrm{vir}}$, in the virgin sate, then the equation in the virgin state is rewritten as

$$\begin{aligned}&\psi^{vir}=\psi_m^{vir}+\psi_{fc}^{vir}+\psi_{fl}^{vir}\\&\psi_m^{vir}=c\left(I_1-3\right),\psi_{fc}^{vir}=\frac{k_1}{2k_2}\left[e^{k_2(I_4-1)^2}-1\right],\psi_{fl}^{vir}=\frac{k_3}{2k_4}\left[e^{k_4(I_6-1)^2}-1\right]\end{aligned}\tag{10}$$

Similarly, the Cauchy stress components in the tissue are divided into three parts: the first part is the stress in the matrix σ_m^{vir} due to ψ_m^{vir}, the second part is the stress in the circumferential fibres σ_{fc}^{vir} and the third part is the stress in the longitudinal fibres σ_{fl}^{vir}, i.e.

$$\begin{aligned}&\sigma_c^{vir}=\sigma_{mc}^{vir}+\sigma_{fc}^{vir},\sigma_l^{vir}=\sigma_{ml}^{vir}+\sigma_{fl}^{vir}\\&\sigma_{mc}^{vir}=\lambda_c\frac{\partial\psi_m^{vir}}{\partial I_1}\frac{\partial I_1}{\partial\lambda_c},\sigma_{fc}^{vir}=\lambda_c\frac{\partial\psi_{fc}^{vir}}{\partial I_4}\frac{\partial I_4}{\partial\lambda_c}\\&\sigma_{ml}^{vir}=\lambda_l\frac{\partial\psi_m^{vir}}{\partial I_1}\frac{\partial I_1}{\partial\lambda_l},\sigma_{fl}^{vir}=\lambda_l\frac{\partial\psi_{fl}^{vir}}{\partial I_6}\frac{\partial I_6}{\partial\lambda_l}\end{aligned}\tag{11}$$

Likewise, the circumferential Young's moduli in total, in the matrix and in the fibres E_c^{dam}, E_{mc}^{dam} and E_{fc}^{dam} as well as the longitudinal Young's moduli in total, in the matrix and in the fibre E_l^{dam}, E_{ml}^{dam} and E_{fl}^{dam} are expressed as

$$\begin{aligned}&E_c^{vir}=\partial\sigma_c^{vir}\big/\partial\lambda_c,E_{mc}^{vir}=\partial\sigma_{mc}^{vir}\big/\partial\lambda_c,E_{fc}^{vir}=\partial\sigma_{fc}^{vir}\big/\partial\lambda_c\\&E_l^{vir}=\partial\sigma_l^{vir}\big/\partial\lambda_l,E_{ml}^{vir}=\partial\sigma_{ml}^{vir}\big/\partial\lambda_l,E_{fl}^{vir}=\partial\sigma_{fl}^{vir}\big/\partial\lambda_l\end{aligned}\tag{12}$$

For linear materials, the damage variable is related to the ratio of the Young's modulus in the damaged state to the modulus in the virgin state, [3, 8, 9, 16, 17, 30, 31], and written mathematically as

$$d=1-E^{dam}\big/E^{vir}\tag{13}$$

For anisotropic, nonlinear GB walls, it is supposed that this definition is held for each pair of Young's moduli in Eq. (9) in the damaged state and those in Eq. (12) in the virgin state. Then the damage variables for GB walls are decided by the following expressions

$$\begin{aligned}&d_c=1-E_c^{dam}\big/E_c^{vir},d_{mc}=1-E_{mc}^{dam}\big/E_{mc}^{vir},d_{fc}=1-E_{fc}^{dam}\big/E_{fc}^{vir}\\&d_l=1-E_l^{dam}\big/E_l^{vir},d_{ml}=1-E_{ml}^{dam}\big/E_{ml}^{vir},d_{fl}=1-E_{fl}^{dam}\big/E_{fl}^{vir}\end{aligned}\tag{14}$$

where d_c represents the global damage degree of GB walls in the circumferential direction, d_{mc} and d_{fc} describe the damage degree in the matrix and fibres in the walls; accordingly, d_l, d_{ml} and d_{fl} reflect the damage degree in total, in the matrix and in the fibres in the longitudinal direction.

The Cauchy stresses, Young's moduli in total, in the matrix and fibres are illustrated in Figs. 6 and 7 for the human and porcine GB walls. In comparison with the stresses and Young's moduli in the fibres, the stresses and Young's moduli in the matrix are so small that they can be neglected for two kinds of GB wall.

In the matrix, the stresses and Young's moduli fail to demonstrate any difference in value in the damaged state from those in the virgin state. In the fibres, however, the stresses and Young's moduli are reduced significantly in the damaged state from the virgin state at a stretch more than 1.15 for the human GB wall and 1.25 for the porcine GB wall. This fact suggests that the damage does occur in the fibres at a high stretch rather in the matrix.

The damage variables estimated by Eq. (14) are presented in Fig. 8 for the human and porcine GB walls. It is clear that two damage variables, d_{mc} and d_{ml} are nearly zero, implying there is no damage effect in the matrix basically. In the fibres, two damage variables, d_{fc} and d_{fl} rise markedly with increasing stretch, suggesting a substantially developed damage there. In consequence, the damage in the fibres attributes to the structure failure in the GB walls, i.e. $d_c \approx d_{fc}$ and $d_l \approx d_{fl}$.

Based on the values of the damage variables, d_c and d_l, the damage effect in the longitudinal direction is more dominant than in the circumferential direction for the human GB wall. However, the dominant damage situation is in the circumferential direction for the porcine GB wall.

Since the tissue damage needs energy to generate cracks, the strain energy of GB walls with damage is always lower than the strain energy in the virgin state, see Fig. 8c and d. Here the strain energy functions in the circumferential and longitudinal specimens are defined as the following

$$\begin{aligned}&\psi_c^{vir}=\psi_m^{vir}+\psi_{fc}^{vir},\psi_l^{vir}=\psi_m^{vir}+\psi_{fl}^{vir}\\&\psi_c^{dam}=\psi_m^{dam}+\psi_{fc}^{dam},\psi_l^{dam}=\psi_m^{dam}+\psi_{fl}^{dam}\end{aligned}\tag{15}$$

From the physics point of view, the value of the strain energy function with damage should be equal to or larger than zero. The zero strain energy occurring after being stretched coincides to the complete structure failure. This means that two stretch components in Eq. (1–8) are not infinite and should be subject to limits. Beyond the limits, the value of the strain energy function is less than zero, which is meaningless in physics.

3.4 Finalised damage model

Based on the results in Sect. 3.3, the damage effect in the matrix is negligible in comparison with the fibres for two kinds of GB walls. Thus, the strain energy function with damage effect in both the matrix and the fibres presented with Eq. (6) can be updated by removing the term for the damage effect in the matrix as follows

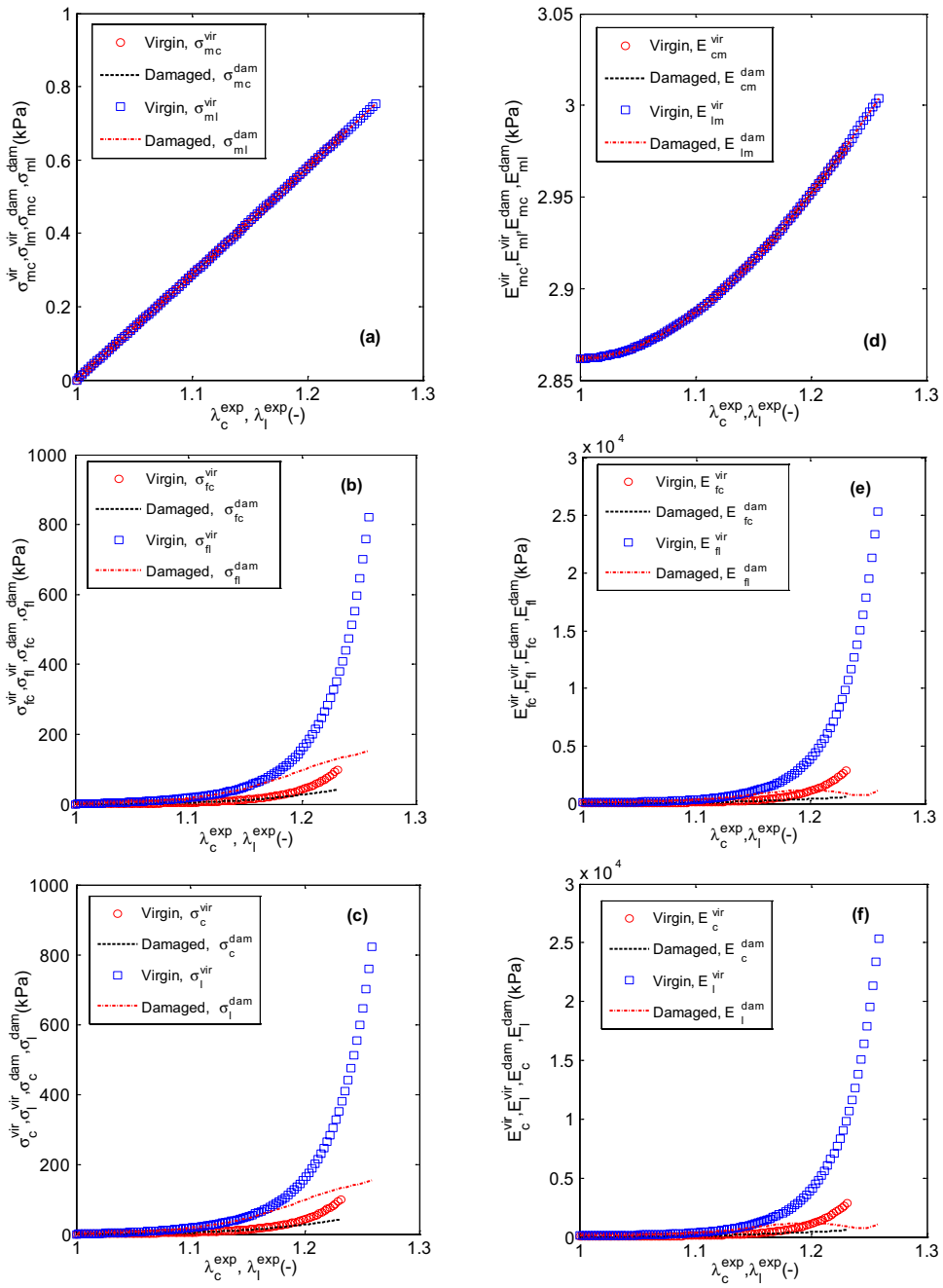

Fig. 6 The Cauchy stresses and Young's moduli in total, in the matrix and fibres for the human GB wall, **a–c** for stresses, **d–f** for Young's moduli

$$\psi^{dam} = c(I_1 - 3) + \frac{k_1}{2k_2}\left\{\exp\left[k_2(I_4 - 1)^2\right] - 1 - \frac{2k_2(I_4 - 1)^{n+2}}{(n+2)(\xi^2 - 1)^n}\right\} + \frac{k_3}{2k_4}\left\{\exp\left[k_4(I_6 - 1)^2\right] - 1 - \frac{2k_4(I_6 - 1)^{n+2}}{(n+2)(\xi^2 - 1)^n}\right\} \tag{16}$$

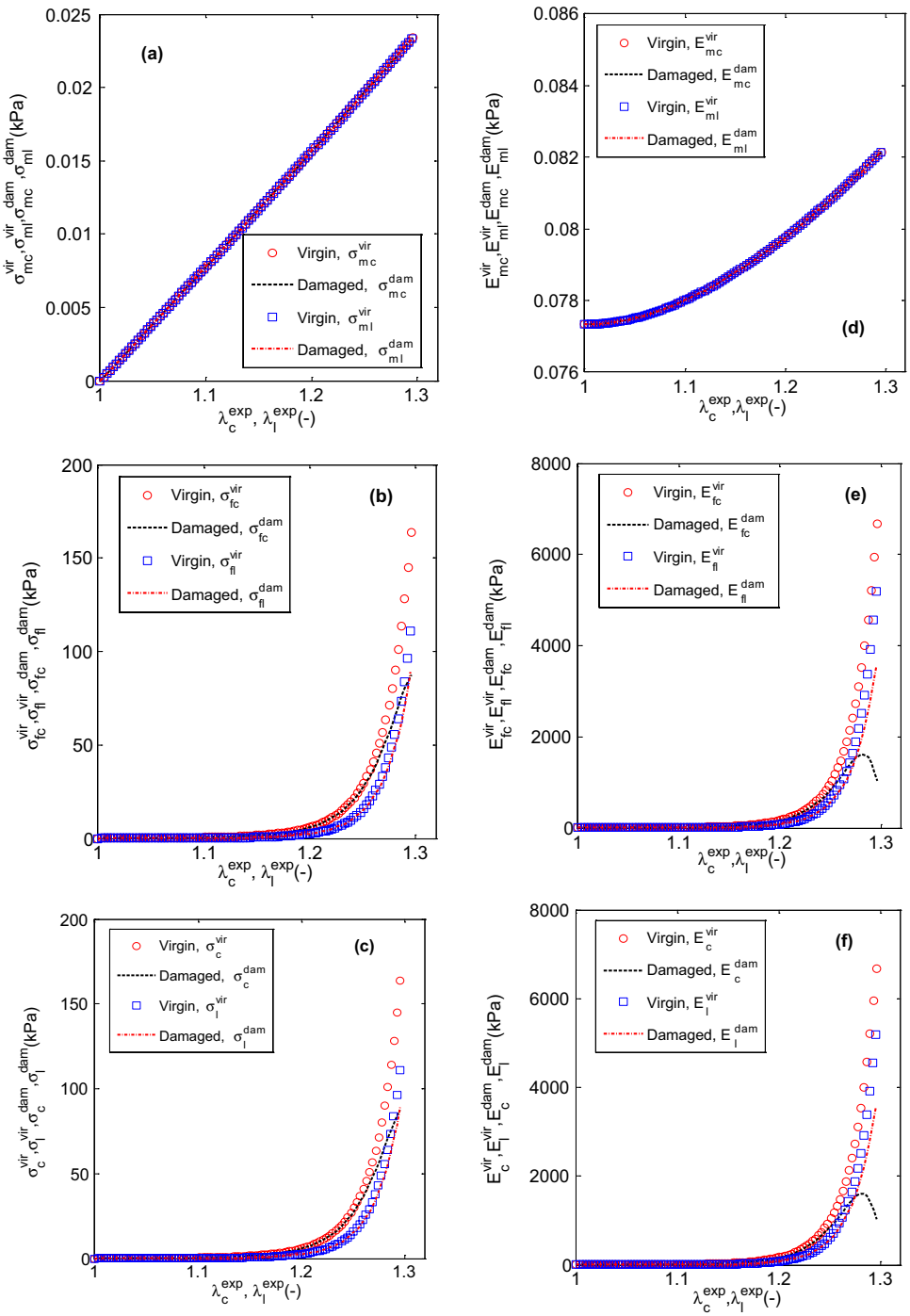

Fig. 7 The Cauchy stresses and Young's moduli in total, in the matrix and fibres for the porcine GB wall, **a–c** for stresses, **d–f** for Young's moduli

The determined model parameters are listed in Table 3. As expected, the values of the parameters and error remain unchanged. Obviously, the updated strain energy function in Eq. (16) is proper for two sets of uniaxial tensile test adopted in the paper.

4 Discussions

For linear materials, under the hypothesis of strain equivalence, scalar damage variable is related to the Young's moduli in undamaged/virgin and damaged states [9, 16, 30, 31]. Particularly, once a brittle material is damaged, its Young's

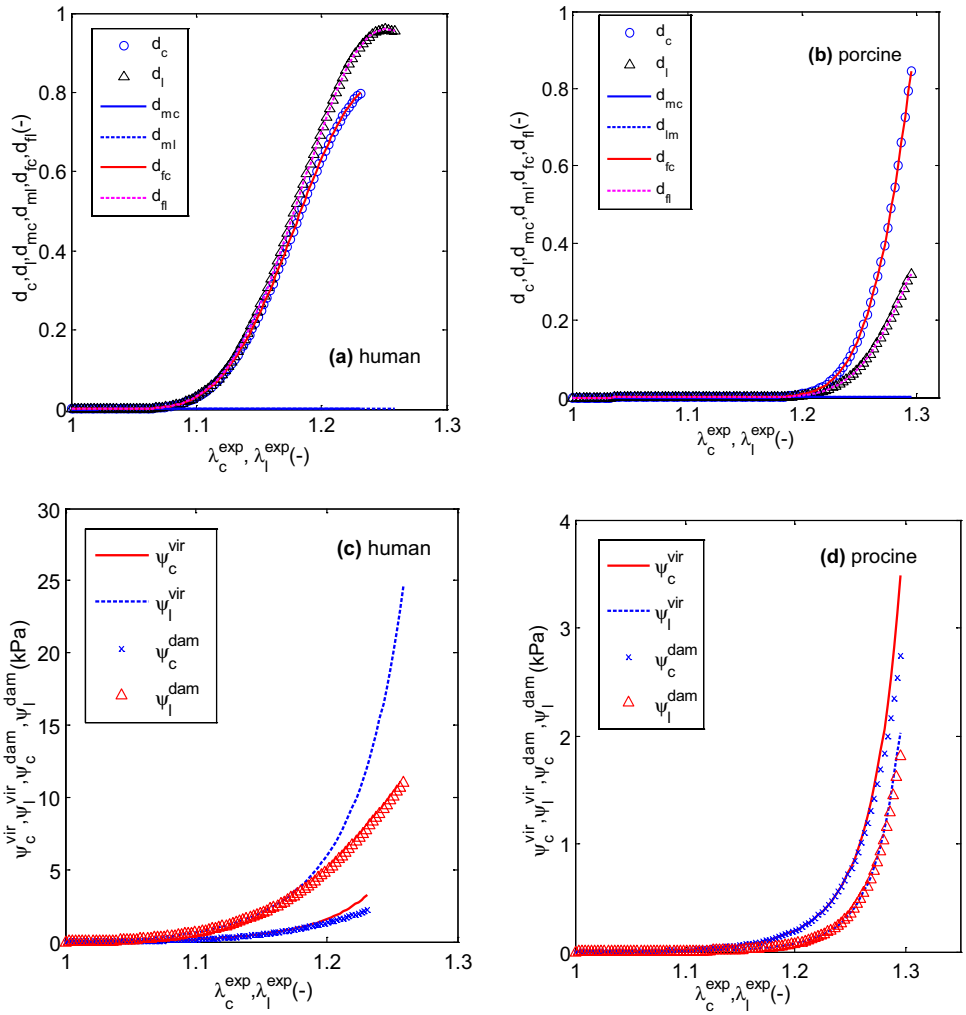

Fig. 8 The damage variables and strain energy of the human and porcine GB walls, **a** and **c** for human, **b** and **d** for porcine

Table 3 Extracted model parameters from uniaxial tensile test data on human and porcine GB walls without damage in matrix but in fibres

Damage effect	Parameter	GB wall	
		Human	Porcine
Included damage effect in fibres only	c (kPa)	0.4770	0.0129
	k_1 (kPa)	5.8311	0.6445
	k_2 (–)	8.9293	10.2208
	k_3 (kPa)	23.8486	0.1964
	k_4 (–)	8.5417	12.0102
	ξ (–)	1.1825	1.2447
	n (–)	7.0763	18.6269
	m (–)	N/A	N/A
	ζ (–)	N/A	N/A
	ε (%)	4.5836	8.1985

modulus must be degraded in comparison with its undamaged state, showing Young's modulus degradation or stress softening effect.

In the paper, for nonlinear anisotropic GB walls, the Cauchy stress-stretch experimental data points of the circumferential and longitudinal specimens were best fitted by using 6th-order polynomial, subsequently, the local/instant Young's moduli of the fitted curves were calculated across the experimental ranges of stretch with the expressions of $E_c^{\exp} = d\sigma_c^{\exp} \Big/ d\lambda_c^{\exp}$ and $E_l^{\exp} = d\sigma_l^{\exp} \Big/ d\lambda_l^{\exp}$. And then, the yield points where the maximum Young's modulus was developed were identified by satisfying the conditions of $dE_c^{\exp} \Big/ d\lambda_c^{\exp} = d^2\sigma_c^{\exp} \Big/ d\lambda_c^{\exp 2} = 0$ and $dE_l^{\exp} \Big/ d\lambda_l^{\exp} = d^2\sigma_l^{\exp} \Big/ d\lambda_l^{\exp 2} = 0$, respectively. When a stretch is beyond these points, the instant Young modulus is degraded, indicating the material is damaged. Finally, the corresponding terms are involved in the strain energy function to take the damage effect into account. This idea hasn't been documented in literature so far.

After pre-conditioning, GB walls exhibited a hyperelastic behaviour without any plastic characteristics [14, 32], suggesting the GB walls with brittle damage. In this sense, the damage variable for isotropic, homogenous and brittle materials [3, 9, 16, 30, 31] was extended into anisotropic homogenous GB walls by introducing a scalar damage variable to the matrix and two families of fibres individually. Such an extension in damage variable for GB walls has not been declared in literature.

Based on the values of these damage variables, the damage states of the matrix and two families of fibres inside a GB wall were estimated. For two pairs of GB wall samples used in the paper, the damage variable of the matrix is zero, but the variables of two families of fibres are greater than zero. Naturally, the damage occurs in the fibres rather than in the matrix. This method for indicating damage state is novel for GB walls.

Honestly, the paper is subject to a few noticeable limitations. Firstly, the number of sets of uniaxial tensile test data is a very limited in literature. Secondly, the evidence of damage pattern inside GB walls supported by microscopical observations remains lacked in the literature as well; hence the method proposed in the paper needs to be updated with new experimental data. Thirdly, the virgin biomechanical properties presented in Figs. 6 and 7 are determined mathematically, and might not be the exactly acutal values of the GB walls. Finally, since the experimental data available are for healthy GBs, the biomechanical properties determined here cannot be correlated to pathology of GB disease. Nonetheless, these limitations need to be removed by employing more advanced experimental tensile data of GB walls in the future.

5 Conclusions

In this contribution, constitutive laws with damage effect were established based on the existing uniaxial tensile test data on the human and porcine GB walls in passive state in literature. The damage effect in the walls was clarified by using the yield points in the experimental Cauchy stress-stretch curves. The model parameters in the constitutive law with damage effect were decided with a custom MATLAB code based on two sets of uniaxial tensile test data. The damage variables were introduced to the matrix and two families of fibres to evaluate the damage degree in the walls. It was identified that the stresses and Young's moduli developed in two families of fibres were so high that the stresses in the matrix could be neglected. The existing strain energy function without damage effect failed to fit the uniaxial tensile test data for GB walls properly, but the strain energy function with the effect could do this quite well. Based on the damage variables evaluated, the damage effect emerged in two families of fibres rather than in the matrix. In the future, attention should be paid to microscopic observations of damage effect on GB walls and experimental study on more GB wall samples including diseased cases.

Compliance with ethical standards

Conflict of interest The author has no conflict of interest.

Ethical approval This article does not contain any studies with human participants or animals performed by the author.

Appendix: Custom MATLAB program for damage model

The damage model described with Eqs. (6)–(15) was encoded in MATLAB by using a main program and a user function. At first, the experimental data of two uniaxial tensile tests presented with the curves in Fig. 2c are read into the main program after the curves were digitalized by employing a digitizer. The lower and upper bounds of nine model constants are specified. To ensure a global optimization process, the lower bound should be small enough while the upper bound should be large enough. Table 4 summarizes the lower and upper bounds applied in the parameter optimization process in the paper. For the model without damage effect the lower and upper bounds of ξ and ζ are 10^8, and those of m and n are 1 to remove their effect on the model and restore the model represented by Eq. (1) without damage, but the bounds of the rest parameter are the same those in the model with damage.

The *lsqnonlin* function in MATLAB was chosen to carry out the parameter optimization by minimizing the objective function Eq. (2). In the *lsqnonlin* function, "trust-region-reflective" optimization algorithm is implanted. In the algorithm, the objective function is approximated with a model function i.e. a quadratic function. Trust region is a subset of the region of the objective function. The minimum objective function is achieved in the trust region. In the trust region algorithm, the search step and size of trust region are decided and updated according to the ratio of the real change of the objective function to the predicted change in the objective function by the model function to ensure sufficient reduction of the objective function. Such procedures can result in the trust region may be out of one bound. Thus, the search direction should be reflected to the interior region constrained by the bounds with the law of reflection in optics on that bound. Compared with Newton method and Levenberg–Marquardt algorithm, the trust-region-reflective algorithm can ensure the optimization iteration remaining in

Table 4 Summary of lower and upper bounds of nine parameters used in their optimization process

Parameter	Bounds		Model type
	Lower	Upper	
c (kPa)	0	10	With damage
k_1 (kPa)	0	50	
k_2 (–)	0	50	
k_3 (kPa)	0	50	
k_4 (–)	0	50	
ξ (–)	1	1.5	
n (–)	0.1	20	
m (–)	0.1	20	
ζ (–)	3	6	
c (kPa)	0	10	Without damage
k_1 (kPa)	0	50	
k_2 (–)	0	50	
k_3 (kPa)	0	50	
k_4 (–)	0	50	
ξ (–)	10^8	10^8	
n (–)	1	1	
m (–)	1	1	
ζ (–)	10^8	10^8	

the strict feasible region and its convergence rate is in the 2nd-order [24].

Nine internal optimization variables in the *lsqnonlin* function $[x_1, x_2, x_3, \ldots, x_9]$ were selected to represent nine parameters $[c, k_1, k_2, k_3, k_4, \xi, n, m, \zeta]$ in the physical domain. However, the variables of $[x_1, x_2, x_3, \ldots, x_9]$ in the computational domain of the *lsqnonlin* function is subject to the same lower bound 0 and upper bound 1, but also the step sizes for searching the optimum solution are identical to all the variable. Thus, a transformation relationship between $[x_1, x_2, x_3, \ldots, x_9]$ in the computational domain and $[c, k_1, k_2, k_3, k_4, \xi, n, m, \zeta]$ in the physical domain is needed. Here a linear relationship is employed and written as the followings

$$\begin{cases} c = c_{\min} + x_1 \times (c_{\max} - c_{\min}) \\ k_1 = k_{1\min} + x_2 \times (k_{1\max} - k_{1\min}) \\ k_2 = k_{2\min} + x_3 \times (k_{2\max} - k_{2\min}) \\ k_3 = k_{3\min} + x_4 \times (k_{3\max} - k_{3\min}) \\ k_4 = k_{4\min} + x_5 \times (k_{4\max} - k_{4\min}) \\ \xi = \xi_{\min} + x_6 \times (\xi_{\max} - \xi_{\min}) \\ n = n_{\min} + x_7 \times (n_{\max} - n_{\min}) \\ m = m_{\min} + x_8 \times (m_{\max} - m_{\min}) \\ \zeta = \zeta_{\min} + x_9 \times (\zeta_{\max} - \zeta_{\min}) \end{cases} \tag{A1}$$

where the lower and upper bounds of nine parameters, such as $c_{\min}$, $c_{\max}$, $k_{1\min}$, $k_{1\max}$ and so on, have been listed in Table 4. Accordingly, the step sizes in the computational domain are related to those in the counterpart in the physical domain by the following from Eq. (A1)

$$\begin{cases} \Delta c = \Delta x_1 \times (c_{\max} - c_{\min}) \\ \Delta k_1 = \Delta x_2 \times (k_{1\max} - k_{1\min}) \\ \Delta k_2 = \Delta x_3 \times (k_{2\max} - k_{2\min}) \\ \Delta k_3 = \Delta x_4 \times (k_{3\max} - k_{3\min}) \\ \Delta k_4 = \Delta x_5 \times (k_{4\max} - k_{4\min}) \\ \Delta \xi = \Delta x_6 \times (\xi_{\max} - \xi_{\min}) \\ \Delta n = \Delta x_7 \times (n_{\max} - n_{\min}) \\ \Delta m = \Delta x_8 \times (m_{\max} - m_{\min}) \\ \Delta \zeta = \Delta x_9 \times (\zeta_{\max} - \zeta_{\min}) \end{cases} \tag{A2}$$

Based on Eq.(A2), even though the step sizes of the internal variables $[x_1, x_2, x_3, \ldots, x_9]$ are the same, i.e. $\Delta x_1 = \Delta x_2 = \Delta x_3 = \cdots = \Delta x_9$ in the *lsqnonlin* function, the step sizes such as Δc, Δk_1, Δk_2, …, $\Delta \zeta$ in the physical domain still vary across the variables.

It was found that $k_1(x_2)$ and $k_3(x_4)$ vary little and affect the optimization results negligibly, but $c(x_1)$ changes significantly during the optimization process. Therefore $k_1(x_2)$ and $k_3(x_4)$ have to be updated by $c(x_1)$ after they were calculated with Eq. (A1) in the following manner

$$\begin{cases} k_1 \times c \Rightarrow k_1 \\ k_3 \times c \Rightarrow k_3 \end{cases} \tag{A3}$$

where k_1 and k_3 in the left-hand side have been determined by Eq. (A1).

Additionally, an initial nine parameters $[c_0, k_{10}, k_{20}, k_{30}, k_{40}, \xi_0, n_0, m_0, \zeta_0]$ are generated randomly in the bounds by using *rand* function of MATLAB in terms of $[x_{10}, x_{20}, x_{30}, \ldots, x_{90}]$ to make sure a global optimization process, i.e.

$$\begin{cases} c_0 = c_{\min} + x_{10} \times (c_{\max} - c_{\min}) \\ k_{10} = k_{1\min} + x_{20} \times (k_{1\max} - k_{1\min}) \\ k_{20} = k_{2\min} + x_{30} \times (k_{2\max} - k_{2\min}) \\ k_{30} = k_{3\min} + x_{40} \times (k_{3\max} - k_{3\min}) \\ k_{40} = k_{4\min} + x_{50} \times (k_{4\max} - k_{4\min}) \\ \xi_0 = \xi_{\min} + x_{60} \times (\xi_{\max} - \xi_{\min}) \\ n_0 = n_{\min} + x_{70} \times (n_{\max} - n_{\min}) \\ m_0 = m_{\min} + x_{80} \times (m_{\max} - m_{\min}) \\ \zeta_0 = \zeta_{\min} + x_{90} \times (\zeta_{\max} - \zeta_{\min}) \end{cases} \tag{A3}$$

where $x_{10} = rand(1, 1)$, $x_{20} = rand(1, 1)$, $x_{30} = rand(1, 1)$, …, $x_{90} = rand(1, 1)$.

The option in the *lsqnonlin* function is as follows: MaxIter = 4000, TolFun = 10^{-8}, TolX = 10^{-8}, Diffminchange = 10^{-4}, Diffmaxchange = 10^{-2} and

MaxFunEvals = 50,000 where MaxIter is maximum number of iterations allowed, TolFun is termination tolerance on the objective function value, TolX is termination tolerance on $[x_1, x_2, x_3, \ldots, x_9]$, Diffminchange and Diffmaxchange are minimum and maximum changes in variables for finite difference derivatives of the objective function, respectively; MaxFunEvals is maximum number of the objective function evaluations allowed.

The temporary nine parameters, stresses and objective function value at the experimental stretches are calculated in the user function. The user function is called repeatedly by the *lsqnonlin* function until a convergent optimization process arrives. The stress-stretch curves, strain energy function values, Young's moduli, damage variables and relevant plots are figured out in the main program based on the determined nine parameters.

References

1. Amaral J, Xiao ZL, Chen Q, et al. Gallbladder muscle dysfunction in patients with chronic acalculous disease. Gastroenterology. 2001;120(2):506–11.
2. Bateson MC. Gallbladdr disease. BMJ. 1999;318:1745–8.
3. Becker W, Gross D. A one-dimensional micromechanical model of elastic-microplastic damage evolution. Acta Mech. 1987;70:221–33.
4. Behar J, Lee KY, Thomson WR, Biancani P. Gallbladder contraction in patients with pigment and cholesterol stones. Gastroenterology. 1989;97:1479–84.
5. Borly L, Hojgaard L, Gronvall S, Stage JG. Human gallbladder pressure and volume: validation of a new direct method for measurements of gallbladder pressure in patients with acute cholecystitis. Clin Physiol Funct Imaging. 1996;16(2):145–56.
6. Brotschi EA, Lamorte WW, Williams LF. Effect of dietary cholesterol and indomethacin on cholelithiasis and gallbladder motility in guinea pig. Dig Dis Sci. 1984;29(11):1050–6.
7. Cerci SS, Ozbek FM, Cerci C, et al. Gallbladder function and dynamics of bile flow in asymptomatic gallstone disease. World J Gastroenterol. 2009;15(22):2763–7.
8. Chaboche JL. Continuum damage mechanics: present state and future trends. Nucl Eng Des. 1987;105:19–33.
9. Fett T, Schell KG, Hoffmann MJ, et al. Effect of damage by hydroxyl generation on strength of silica fibers. J Am Ceram Soc. 2018. https://doi.org/10.1111/jace.15508.
10. Fung YC, Fronek K, Patitucci P. Pseudoelasticity of arteries and the choice of its mathematical expression. Am J Physiol. 1979;237(5):H620–31.
11. Genovese K, Casaletto L, Humphrey JD, et al. Digital image correlation-based point-wise inverse characterization of heterogeneous material properties of gallbladder in vitro. Proc R Soc Ser A. 2014;470:20140152.
12. Goussous N, Kowdley GC, Sardana N, et al. Gallbladder dysfunction: how much longer will it be controversial? Digestion. 2014;90:147–54.
13. Holzapfel GA, Gasser TC, Ogden RW. A new constitutive framework for arterial wall mechanics and a comparative study of material models. J Elast. 2000;61(1):1–48.
14. Karimi A, Shojaei A, Tehrani P. Measurement of the mechanical properties of the human gallbladder. J Med Eng Technol. 2017;41(7):541–5.
15. Kurtz RC. Progress in understanding acalculous gallbladder disease. Gastroenterology. 2001;120(2):570–2.
16. Lemaitre J. How to use damage mechanics. Nucl Eng Des. 1984;80:233–45.
17. Lemaitre J, Dufailly J. Damage measurements. Eng Fract Mech. 1987;28:643–61.
18. Matsuki Y. Spontaneous contractions and the visco-elastic properties of the isolated guinea-pig gall-bladder. Jpn J Smooth Muscle Res. 1985;21:71–8.
19. Matsuki Y. Dynamic stiffness of the isolated Guinea-pig gallbladder during contraction induced by cholecystokinin. Jpn J Smooth Muscle Res. 1985;21:427–38.
20. Mahadevan V. Anatomy of the gallbladder and bile ducts. Surgery. 2014. https://doi.org/10.1016/j.mpsur.2014.10.003.
21. Miura K, Saito S. Visco-elastic properties of the gallbladder in rabbit and guinea-pig. J Showa Med Assoc. 1967;27(2):135–8.
22. Li WG, Hill NA, Ogden RW, et al. Anistropic behaviour of human gallbldder walls. J Mech Behav Biomed Mater. 2013;20:363–75.
23. Li WG, Luo XY. An invariant-based damage model for human and animal skins. Ann Biomed Eng. 2016;44:3109–22.
24. Li Y. Trust region, reflective techniques for nonlinear minimization subject to bounds, technical report-CTC93TR152, Cornell Theory Center, Cornell University; 1993.
25. Portincasa P, Di Ciaula A, van Berge-Hengouwen GP. Smooth muscle function and dysfunction in gallbladder disease. Curr Gastroenterol Rep. 2004;6(2):151–62.
26. Rosen J, Brown JD, De S, et al. Biomechanical properties of abdominal organs in vivo and postmortem under compression loads. J Biomech Eng. 2008;130:021020.
27. Ryan J, Cohen S. Gallbladder pressure-volume response to gastrointestinal hormones. Am J Physiol. 1976;230(6):1461–5.
28. Schoetz DJ, LaMorte WW, Wise WE, et al. Mechanical properties of primate gallbladder: description by a dynamic method. Am J Physiol Gastrointest Liver Physiol. 1981;241:G376–81.
29. Stinton LM, Shaffer EA. Epidemiology of gallbladder disease: cholelithiasis and cancer. Gut Liver. 2012;6(2):172–87.
30. Voyiadjis GZ, Kattan PI. On the theory of elastic undamageable materials. J Eng Mater Technol. 2013;135:021002.
31. Voyiadjis GZ, Kattan PI. Decomposition of elastic stiffness degradation in continuum damage mechanics. J Eng Mater Technol. 2017;139:021005.
32. Xiong L, Chui CK, Teo CL. Reality based modelling and simulation of gallbladder shape deformation using variational methods. Int J Comput Assist Radiol Surg. 2013;8:857–65.